Received: 21 October 2018 | Revised: 14 May 2019 | Accepted: 17 June 2019 | Published on: 24 July 2019

DOI: 10.1002/num.22410

RESEARCH ARTICLE

WILEY

Numerical approximation of the generalized regularized long wave equation using Petrov–Galerkin finite element method

Samir Kumar Bhowmik[1] | **Seydi B. G. Karakoc**[2]

[1]Department of Mathematics, University of Dhaka, Dhaka, Bangladesh
[2]Department of Mathematics, Faculty of Science and Art, Nevsehir Haci Bektas Veli University, Nevsehir, Turkey

Correspondence
Samir Kumar Bhowmik, Department of Mathematics, University of Dhaka, 1000 Dhaka, Bangladesh.
Email: bhowmiksk@gmail.com; bhowmiksk@du.ac.bd

Abstract

The generalized regularized long wave (GRLW) equation has been developed to model a variety of physical phenomena such as ion-acoustic and magnetohydrodynamic waves in plasma, nonlinear transverse waves in shallow water and phonon packets in nonlinear crystals. This paper aims to develop and analyze a powerful numerical scheme for the nonlinear GRLW equation by Petrov–Galerkin method in which the element shape functions are cubic and weight functions are quadratic B-splines. The proposed method is implemented to three reference problems involving propagation of the single solitary wave, interaction of two solitary waves and evolution of solitons with the Maxwellian initial condition. The variational formulation and semi-discrete Galerkin scheme of the equation are firstly constituted. We estimate rate of convergence of such an approximation. Using Fourier stability analysis of the linearized scheme we show that the scheme is unconditionally stable. To verify practicality and robustness of the new scheme error norms L_2, L_∞ and three invariants I_1, I_2, and I_3 are calculated. The computed numerical results are compared with other published results and confirmed to be precise and effective.

KEYWORDS

cubic B-splines, GRLW equation, Petrov–Galerkin, solitary waves, soliton

1 | INTRODUCTION

The generalized regularized long wave (GRLW) equation was originated by a famous nonlinear analyst Peregrine who first successfully introduced the RLW equation as a perfect alternative to the famous

Korteweg–de Vries (KdV) equation for studying soliton phenomena and as a mathematical model for small amplitude long waves on the surface of water [1]. Nonlinear evolution equations play fundamental roles in various fields of science mostly in physics, applied mathematics, and in engineering problems. Analytical solutions of these equations are commonly not derivable, particularly when the nonlinear terms are contained. Numerical solutions of these equations are very practical to analyze the physical phenomena due to the fact that analytical solutions of these equations are found for the restricted boundary and initial conditions. The RLW equation

$$u_t + u_x + auu_x - bu_{xxt} = 0, \tag{1}$$

is one of the important model in physics media on account of it defines phenomena with weak nonlinearity and dispersion waves, involving nonlinear transverse waves in shallow water, ion-acoustic waves in plasma, hydromagnetic wave in cold plasma, plasma, elastic media, optical fibers, acoustic-gravity waves in compressible fluids, pressure waves in liquid–gas bubbles and acoustic waves inharmonic crystals. The solutions of this equation are sorts of solitary waves called as solitons whose form are not affected by a collision. It was first alleged by Peregrine [1, 2] for studying soliton phenomena and as a sample for small-amplitude long-waves on the surface of water in a channel and widely studied by Benjamin et al. [3]. In physical situations such as unidirectional waves propagating in a water channel, long-crested waves in near-shore zones, and many others, the RLW equation serves as an alternative model to the KdV equation [4, 5]. An exact solution of the equation was obtained under the limited initial and boundary conditions in [6] for this reason it got fascinate from a numerical point of view. Therefore, numerical solutions of the RLW equation have been the matter of many papers. Various effective methods have been presented to solve the equation such as finite difference method [7–10], pseudo-spectral method [11], meshfree method [12], Adomian decomposition method [13] and various forms of finite element methods in [14–17]. Indeed, the RLW equation is a special case of the GRLW equation which is an alternative to the KdV equation for describing nonlinear dispersive waves and can be used to characterize phenomena with weak nonlinearity and dispersion waves. It is defined as

$$u_t + u_x + p(p+1)u^p u_x - \mu u_{xxt} = 0, \quad (x,t) \in \Omega \times (0,T], \tag{2}$$

subject to some suitable initial and boundary conditions where p is a positive integer, μ is positive constant. Some physical boundary conditions require u that $u \to 0$ for $x \to \partial\Omega$. In Equation (2) u indicates dimensionless surface elevation, x distance and t time. On the other hand, the GRLW equation has received much less attention, presumably because of its higher nonlinearity for $p > 2$ and the fact that it possesses a finite number of conserved quantities and admits solitary waves as solutions, but, unlike other equations, the stability of its solutions depends on their velocity [18]. Some solitary wave solutions for GRLW equations have been obtained by Hamdi et al. [19] and Ramos [20] studied solitary wave interactions based on the separation of the temporal and spatial derivatives. Zhang [21] implemented finite difference method for a Cauchy problem while Kaya [13], Kaya and El-Sayed [22] indicated the numerical solution of the GRLW equation by using the Adomian decomposition method. Roshan [23] have procured numerical solutions of the GRLW equation by the application of Petrov–Galerkin method, which uses a linear hat function as the trial function and a quintic B-spline function as the test function. Wang et al. [24] offered a mesh-free method for the GRLW equation based on the moving least-squares approximation. Karakoç [25] and Zeybek [26] have obtained solitary-wave solutions of the GRLW equation by using septic B-spline collocation and cubic B-spline lumped Galerkin method. Numerical solutions of the GRLW equation have been obtained by Soliman [27] using He's variational iteration method. Mokhtari and Mohammadi [28] suggested the Sinc-collocation method for this equation. A time-linearization method that uses a Crank–Nicolson procedure in time and three point, fourth-order accurate in space, compact difference equations, is

presented and used to determine the solutions of the GRLW equation and a modified version thereof (mGRLW) by García-López and Ramos [29]. The another special case of the GRLW equation is the modified-RLW (MRLW) equation for $p = 2$. MRLW equation was solved numerically by various methods [30–36]. We would refer [37–42] for an application for such models of nonlinear dispersive equations.

Spline functions are a class of piecewise polynomials which provide continuity features being subject to the degree of the polynomials. They are spectacular mathematical instrument for numerical approximations because of their numerous popular specialties. One kind of splines, noted as B-splines, has been used in obtaining the numerical solution of the GRLW equation [25, 26, 31, 32, 43, 44]. Assemblies of B-splines are used as trial functions in the Petrov–Galerkin methods. Especially, cubic B-splines associated with finite element methods have been verified to give very smooth solutions, and use of the cubic B-splines as shape functions in the finite element method warranties continuity of the first and second-order derivatives of trial solutions at the mesh points [15].

In this study, we have designed a lumped Petrov–Galerkin method for the GRLW equation using cubic B-spline function as element shape function and quadratic B-spline function as the weight function. The plan of this paper is as follows:

- In Section 2, the governing equation and its variational formulation and newly established theorems are presented.
- A semi-discrete Galerkin scheme of the equation is notified in Section 3.
- In Section 4, a lumped Petrov–Galerkin finite element technique has been practiced to GRLW equation. Resulting system can be solved with a sort of the Thomas algorithm.
- Section 5 is dedicated to stability analysis of the method.
- The results of numerical examples are reported in Section 6. The last section is a brief conclusion.

2 | VARIATIONAL FORMULATION AND ENERGY ESTIMATES

Here we are dedicated to write the initial-boundary value problem in a variational form, and use this weak form to derive some estimates for its solution. We start by proving existence and uniqueness of solutions by using this variational form. The higher order nonlinear space time dependent partial differential equation (2) can be written as

$$u_t - \mu \Delta u_t = \nabla \mathcal{F}(u), \quad (x,t) \in \Omega \times (0,T] \tag{3}$$

where $\mathcal{F}(u) = -u(1+pu^p)$, subject to the initial condition

$$u(x,0) = f_1(x), \quad x \in \Omega, \tag{4}$$

and the boundary conditions

$$u(x,t) = 0, \quad (x,t) \in \partial\Omega \times (0,T]. \tag{5}$$

In order to define the weak form of the solutions of (3) and to examine the existence and uniqueness of the weak solutions we define the following spaces.

Here $H^k(\Omega)$, $k \geq 0$ (integer) is an usual normed space of real valued functions on Ω and

$$H_0^k(\Omega) = \left\{ v \in H^k(\Omega) : \frac{\partial^j v}{\partial v^j} = 0 \text{ on } \partial\Omega,\ i = 0, 1, \dots, k-1 \right\},$$

and the norm on the space is denoted by $\|\cdot\|_k$ which is the usual H^k norm, and when $k = 0$ $\|\cdot\|_0 = \|\cdot\|$ represents the well known L_2 norm and $(\cdot,\cdot)$ represents L_2 inner product [45].

Multiplying (3) by $\xi \in H_0^1(\Omega)$, and then integrating over Ω we have

$$(u_t, \xi) - \mu(\Delta u_t, \xi) = (\nabla \mathcal{F}(u), \xi).$$

Applying Green's theorem on the above integral we opt to find $u(\cdot, t) \in H_0^1$ so that

$$(u_t, \xi) + \mu(\nabla u_t, \nabla \xi) = -(\mathcal{F}(u), \nabla \xi), \quad \forall \ \xi \in H_0^1, \tag{6}$$

with $u(0) = u_0$.

Theorem 1 *If u is a solution of* (6) *then*

$$\|u(t)\|_1 = \|u_0\|_1, \quad t \in (0, T], \quad \text{and} \quad \|u\|_{L^\infty(L^\infty(\Omega))} \leq C\|u_0\|_1$$

holds if $u_0 \in H_0^1$, and C is a positive constant.

Proof. Replacing $\xi \in H_0^1$ by $u \in H_0^1$ in (6) results

$$(u_t, u) + \mu(\nabla u_t, \nabla u) = -(\mathcal{F}(u), \nabla u) \tag{7}$$

with $u(0) = u_0$ which gives

$$\frac{1}{2}\frac{d}{dt}[\|u\|^2 + \mu\|\nabla u\|^2] = \int_\Omega u[\nabla \cdot \mathcal{F}(u)]dx. \tag{8}$$

Now

$$u\nabla \cdot \mathcal{F}(u) = \nabla \cdot [\mathcal{F}(u)u] - \nabla \cdot [\mathcal{G}(u)],$$

if $u \in H_0^1$ where $\mathcal{G}\prime(u) = \mathcal{F}(u)$. For the simplicity of the analysis from now on in this section we fix $\mu = 1$. The analysis for a general μ is the similar. Also, from the boundary conditions in (7) we have $u = 0$ on $\partial\Omega$ and so $\mathcal{G}(0) = 0$, and then

$$\int_\Omega u[\nabla \cdot \mathcal{F}(u)]dx = \int_\Omega \nabla(u\mathcal{F}(u))dx = 0.$$

Thus (8) yields

$$\frac{1}{2}\frac{d}{dt}(\|u\|_1^2) = 0,$$

and so

$$\|u\|_1^2 = \|u_0\|_1^2,$$

confirms the proof of first part. The proof of second part follows from Sobolev embedding theorem [45, 46]. ∎

Theorem 2 *A unique solution of* (6) *exists for any $T > 0$ such that*

$$u \in L^\infty(0, T, H_0^1(\Omega)) \ \text{ where } \ (u(x, 0), \xi) = (u_0, \xi), \xi \in H_0^1(\Omega),$$

if $u_0 \in H_0^1$ for any $T > 0$.

Proof. In order to prove the uniqueness of the solution of (6) we consider an orthogonal basis $\{w_i\}_{i=1}^\infty$ for $H_0^1(\Omega)$ and

$$v^m = span\{w_1, w_2, \ldots, w_m\}.$$

Now we define

$$u^m(t) = \sum_{i=1}^{m} c_i(t) w_i,$$

for each $t > 0$ to satisfy

$$(u_t^m, \xi) + (\nabla u_t^m, \nabla \xi) = -(\mathcal{F}(u^m), \nabla \xi), \quad \forall \ \xi \in v^m, \tag{9}$$

with $u^m(0) = u_{0,\,m}$ where

$$u_{0,m} = u^m(0) = \sum_{i=1}^{m} c_i(0) w_i = P^m u_0.$$

Here P^m is an orthogonal projection onto finite dimensional space v^m, and $u_{0,m} \to u_0 \in H_0^1(\Omega)$ [45, 46]. Hence the weak form (9) can be written as a system of first order nonlinear ordinary differential equation and there exist a positive time $t_m > 0$ such that the nonlinear system of differential equations has a unique solution u^m over $(0, t_m)$.

Also from Theorem 1 it is easy to see that

$$\|u^m\|_\infty \leq C \|u_0\|_1$$

and

$$\|\mathcal{F}(u^m)\|^2 \leq C \|u_0\|_1^2$$

which shows that $\mathcal{F}(u^m)$ is bounded in $L^\infty(0, T, L_2(\Omega))$. Now by setting $\xi = u_t^m$ in (9)

$$(u_t^m, u_t^m) + (\nabla u_t^m, \nabla u_t^m) = -(\mathcal{F}(u^m), \nabla u_t^m).$$

Thus

$$\|u_t^m\|_1^2 = -(\mathcal{F}(u^m), \nabla u_t^m)$$

which yields

$$\|u_t^m\|_1 \leq C \|u_0\|_1.$$

Hence $\{u^m\}$ and $\{u_t^m\}$ are uniformly bounded in $L^\infty(0, T, H_0^1(\Omega))$.

By setting $\xi = w_i$ in (9) we have

$$(u_t^m, w_i) + (\nabla u_t^m, \nabla w_i) = -(\mathcal{F}(u^m), \nabla w_i).$$

Thus the existence of solutions of the problem follows from the denseness of $\{w_i\}$ in $H_0^1(\Omega)$.

Considering u and v as two solutions of (6) with $u(0) = 0$ and $v(0) = 0$, we define $W = u - v$. Then $W(0) = 0$. Also

$$(W_t^m, \xi) + (\nabla W_t^m, \nabla \xi) = -(\mathcal{F}(W^m), \nabla \xi).$$

Replacing ξ by W in the above equation and following the boundedness of u and v one obtains [45, 47]

$$\frac{d}{dt} \|W\|_1 \leq C \|W\|_1.$$

Integrating the above inequality over $[0, t]$ yields

$$\|W\|_1 \leq \|W(0)\|_1 + C \int_0^t \|W\|_1 \, ds.$$

Now applying Gronwall's Lemma it is easy to see that

$$\|W\|_1 \leq e^{Ct}\|W(0)\|_1 = 0,$$

which confirms $W = 0$ completes the proof [45, 47]. ■

3 | THE SEMIDISCRETE GALERKIN B-SPLINE FINITE ELEMENT METHOD

Consider $0 < h < 1$. A finite dimensional subspace S_h of $H_0^1(\Omega)$ is considered such that for $u \in H_0^1(\Omega) \cap H^4(\Omega)$, there exists a constant C independent of h [45–47] such that

$$\inf_{\xi \in S_h} (\|u - \xi\| + \|u - \xi\|_1) \leq Ch^4. \tag{10}$$

Here we aim to find solutions of a semi-discrete formulation of (3) $u_h : [0, T] \to S_h$ such that

$$(u_{ht}, \xi) + (\nabla u_{ht}, \nabla \xi) = -(\mathcal{F}(u_h), \nabla \xi), \quad \xi \in S_h, \tag{11}$$

with $u_h(0) = u_{0,h} \in S_h$ is an approximation of u_0. Before proving the original accuracy result we first establish a priori bound of the approximate solution of (11) below.

Theorem 3 *The solution $u_h \in S_h$ of* (11) *satisfies*

$$\|u_h\|_1^2 = \|u_{0,h}\|_1^2, \quad t \in (0, T],$$

and

$$\|u_h\|_{L^\infty(L^\infty(\Omega))} \leq C\|u_{0,h}\|_1$$

holds where C is a positive constant.

Proof. The proof is trivial from our discussion in the previous section (Theorem 1). ■

Now we move onto establish the theoretical bound of the error in the semi-discrete Scheme (11) of (6).

To that end we consider the following bilinear form

$$A(u, v) = (\nabla u, \nabla v), \quad \forall \ u, \quad v \in H_0^1,$$

which satisfies the boundedness property

$$| A(u, v) | \leq M\|u\|_1\|v\|_1, \forall \ u, \quad v \in H_0^1 \tag{12}$$

and coercivity property (on Ω)

$$A(u, u) \geq \alpha\|u\|_1, \forall \ u \in H_0^1, \quad \text{for some } \alpha \in \mathbb{R}. \tag{13}$$

Here A satisfies

$$A(u - \widetilde{u}, \xi) = 0, \quad \xi \in S_h, \tag{14}$$

where $\widetilde{u}$ is an auxiliary projection of u [45–47]. Now the accuracy result in such a semi-discrete approximation (11) of (6) can be established by the following theorem.

Theorem 4 *Let $u_h \in S_h$ satisfies* (11) *and $u \in H_0^1(\Omega)$ be that of* (6)*, then the inequality below holds*

$$\|u - u_h\| \leq Ch^4,$$

where $C > 0$ if $\theta(0) = 0$ hold.

Proof. Considering $e = u - u_h$ we write

$$e = \nu + \theta, \qquad \text{where } \nu = u - \widetilde{u} \text{ and } \theta = \widetilde{u} - u_h.$$

Here

$$\begin{aligned}\alpha\|u - \widetilde{u}\|_1^2 &\leq A(u - \widetilde{u}, u - \widetilde{u}) \\ &= A(u - \widetilde{u}, u - \xi), \quad \xi \in S_h, \text{from (13) and (14).}\end{aligned}$$

Also It follows from (12) and (14) and [47] that

$$\|u - \widetilde{u}\|_1 \leq \inf_{\xi \in S_h} \|u - \xi\|_1. \tag{15}$$

So (10) and (15) confirms the following inequalities

$$\|\nu\|_1 \leq Ch^3\|u\|_4, \text{ and } \|\nu\| \leq Ch^4\|u\|_4.$$

Applying $\partial/\partial t$ on (14) and having some simplifications yields [47]

$$\|\nu_t\| \leq Ch^4\|u_t\|_4.$$

Also subtracting (11) from (6) it is easy to see that

$$(\theta_t, \xi) + (\nabla\theta_t, \nabla\xi) = -(\nu_t, \xi) - (\mathcal{F}(u) - \mathcal{F}(u_h), \nabla\xi). \tag{16}$$

Now substituting $\xi = \theta$ in (16), and then applying Cauchy–Schwarz inequality one gets

$$\frac{1}{2}\frac{d}{dt}\|\theta\|_1^2 \leq \|\nu_t\|\|\theta\| + \|\mathcal{F}(u) - \mathcal{F}(u_h)\|\|\nabla\theta\|.$$

Here

$$\|\mathcal{F}(u) - \mathcal{F}(u_h)\| \leq C(\|\nu\| + \|\theta\|),$$

comes from Lipschitz conditions and boundedness of u and u_h and thus

$$\frac{d}{dt}\|\theta\|_1^2 \leq C(\|\nu_t\|^2 + \|\nu\|^2 + \|\theta\|^2 + \|\nabla\theta\|^2).$$

So

$$\|\theta\|_1^2 \leq \|\theta(0)\|_1^2 + C\int_0^t (\|\nu_t\|^2 + \|\nu\|^2 + \|\theta\|^2 + \|\nabla\theta\|^2)dt.$$

Hence Gronwall's lemma, bounds of ν and ν_t confirms

$$\|\theta\|_1 \leq C(u)h^4,$$

if $\theta(0) = 0$, completes the proof [46, 47]. ∎

4 | NUMERICAL IMPLEMENTATIONS OF THE SCHEME

For numerical implementation we restrict ourselves in one space dimension only and we consider $\Omega \subset \mathbb{R}$. To be specific the solution domain is limited to a finite interval $a \leq x \leq b$. Partition the interval $[a, b]$ at points by x_m where $a = x_0 < x_1 < \cdots < x_N = b$ and let $h = (b - a)/N$, $m = 0, 1, 2, \ldots, N$. On

this partition, we shall need the following cubic B-splines $\phi_m(x)$ at the points x_m, $m = 0, 1, 2, \ldots, N$. The cubic B-spline functions $\phi_m(x)$, $(m = -1(1)\, N+1)$ are identified as follows [48]

$$\phi_m(x) = \frac{1}{h^3}\begin{cases} (x - x_{m-2})^3, & x \in [x_{m-2}, x_{m-1}), \\ h^3 + 3h^2(x - x_{m-1}) + 3h(x - x_{m-1})^2 - 3(x - x_{m-1})^3, & x \in [x_{m-1}, x_m), \\ h^3 + 3h^2(x_{m+1} - x) + 3h(x_{m+1} - x)^2 - 3(x_{m+1} - x)^3, & x \in [x_m, x_{m+1}), \\ (x_{m+2} - x)^3, & x \in [x_{m+1}, x_{m+2}], \\ 0 & \text{otherwise.} \end{cases} \tag{17}$$

We search the approximation solution $u_N(x, t)$ to the exact solution $u(x, t)$ which uses these cubic B-splines as trial functions

$$u_N(x, t) = \sum_{j=-1}^{N+1} \phi_j(x)\delta_j(t), \tag{18}$$

where $\delta_j(t)$ are time depended quantities or the nodal parameters to be detected from boundary and weighted residual conditions. Applying the following transformation

$$h\eta = x - x_m \quad 0 \le \eta \le 1, \tag{19}$$

the finite interval $[x_m, x_{m+1}]$ is turned into more easily practicable interval [0, 1]. Therefore cubic B-spline shape functions (17) depending on variable η on the region [0, 1] rearranged with

$$\begin{aligned} \phi_{m-1} &= (1 - \eta)^3, \\ \phi_m &= 1 + 3(1 - \eta) + 3(1 - \eta)^2 - 3(1 - \eta)^3, \\ \phi_{m+1} &= 1 + 3\eta + 3\eta^2 - 3\eta^3, \\ \phi_{m+2} &= \eta^3. \end{aligned} \tag{20}$$

All splines, apart from $\phi_{m-1}(x)$, $\phi_m(x)$, $\phi_{m+1}(x)$, $\phi_{m+2}(x)$ and their four principal derivatives are null over the region [0, 1]. Thereby variation of $u(x, t)$ over [0, 1] is approximated by

$$u_N(\eta, t) = \sum_{j=m-1}^{m+2} \delta_j \phi_j, \tag{21}$$

where $\delta_{m-1}, \delta_m, \delta_{m+1}, \delta_{m+2}$ and B-spline element functions $\phi_{m-1}, \phi_m, \phi_{m+1}, \phi_{m+2}$ as element shape functions. The nodal values u and its derivatives up to second order at the knots x_m are given in terms of the parameters δ_m from the use of the B-splines (20) and the trial solution (21):

$$\begin{aligned} u_m &= u(x_m) = \delta_{m-1} + 4\delta_m + \delta_{m+1}, \\ u'_m &= u'(x_m) = 3(-\delta_{m-1} + \delta_{m+1}), \\ u''_m &= u''(x_m) = 6(\delta_{m-1} - 2\delta_m + \delta_{m+1}). \end{aligned} \tag{22}$$

We take the weight functions Φ_m as quadratic B-splines. The quadratic B-splines Φ_m at the knots x_m are defined as [48]:

$$\Phi_m(x) = \frac{1}{h^2}\begin{cases} (x_{m+2} - x)^2 - 3(x_{m+1} - x)^2 + 3(x_m - x)^2, & x \in [x_{m-1}, x_m), \\ (x_{m+2} - x)^2 - 3(x_{m+1} - x)^2, & x \in [x_m, x_{m+1}), \\ (x_{m+2} - x)^2, & x \in [x_{m+1}, x_{m+2}), \\ 0 & \textit{otherwise}. \end{cases} \tag{23}$$

When we take into consideration of the transformation (19), quadratic B-splines Φ_m are written as

$$\begin{aligned}\Phi_{m-1} &= (1-\eta)^2,\\ \Phi_m &= 1+2\eta-2\eta^2,\\ \Phi_{m+1} &= \eta^2.\end{aligned} \tag{24}$$

Performing the Petrov–Galerkin method to Equation (2) the weak form of Equation (2) is attained as

$$\int_a^b \Phi(u_t + u_x + p(p+1)u^p u_x - \mu u_{xxt})dx = 0. \tag{25}$$

For a unique element $[x_m, x_{m+1}]$ using (19) into Equation (25) we obtain the following integral equation:

$$\int_0^1 \Phi\left(u_t + \frac{1}{h}u_\eta + \frac{p(p+1)}{h}\widehat{u}^p u_\eta - \frac{\mu}{h^2}u_{\eta\eta t}\right)d\eta = 0, \tag{26}$$

where $\widehat{u}$ is accepted as a constant over an element to ease the integral, and Integrating (26) by parts and then using (2) yields:

$$\int_0^1 [\Phi(u_t + \lambda u_\eta) + \beta\Phi_\eta u_{\eta t}]d\eta = \beta\Phi u_{\eta t}\Big|_0^1, \tag{27}$$

where $\lambda = \frac{1+p(p+1)\widehat{u}^p}{h}$ and $\beta = \frac{\mu}{h^2}$. Assuming the weight function Φ_i with quadratic B-spline shape functions given by Equation (23) and substituting (21) into (27), we get the element contributions in the form:

$$\sum_{j=m-1}^{m+2}\left[\left(\int_0^1 \Phi_i\phi_j + \beta\Phi_i'\phi_j'\right)d\eta - \beta\Phi_i\phi_j'\Big|_0^1\right]\dot{\delta}_j^e + \sum_{j=m-1}^{m+2}\left(\lambda\int_0^1 \Phi_i\phi_j' d\eta\right)\delta_j^e = 0, \tag{28}$$

where $\delta^e = (\delta_{m-1}, \delta_m, \delta_{m+1}, \delta_{m+2})^T$ are the element parameters and dot states differentiation to t which can be written in matrix form as follows:

$$[A^e + \beta(B^e - C^e)]\dot{\delta}^e + \lambda D^e\delta^e = 0. \tag{29}$$

The element matrices $A_{ij}^e, B_{ij}^e, C_{ij}^e$ and D_{ij}^e are rectangular 3×4 given by the following integrals;

$$A_{ij}^e = \int_0^1 \Phi_i\phi_j d\eta = \frac{1}{60}\begin{bmatrix}10 & 71 & 38 & 1\\ 19 & 221 & 221 & 19\\ 1 & 28 & 71 & 10\end{bmatrix},$$

$$B_{ij}^e = \int_0^1 \Phi_i'\phi_j' d\eta = \frac{1}{2}\begin{bmatrix}3 & 5 & -7 & -1\\ -2 & 2 & 2 & -2\\ -1 & -7 & 5 & 3\end{bmatrix},$$

$$C_{ij}^e = \Phi_i\phi_j'|_0^1 = 3\begin{bmatrix}1 & 0 & -1 & 0\\ 1 & -1 & -1 & 1\\ 0 & -1 & 0 & 1\end{bmatrix},$$

$$D_{ij}^e = \int_0^1 \Phi_i\phi_j' d\eta = \frac{1}{10}\begin{bmatrix}-6 & -7 & 12 & 1\\ -13 & -41 & 41 & 13\\ -1 & -12 & 7 & 6\end{bmatrix}$$

where i takes the values 1, 2, 3 and the j takes the values $m-1, m, m+1, m+2$ for the typical element $[x_m, x_{m+1}]$. A lumped value for u is obtained from $\left(\frac{u_m+u_{m+1}}{2}\right)^p$ as

$$\lambda = \frac{1+p(p+1)}{2^p h}(\delta_{m-1} + 5\delta_m + 5\delta_{m+1} + \delta_{m+2})^p.$$

Combining contributions from all elements induces to the following matrix equations

$$[A + \beta(B - C)]\dot{\delta} + \lambda D\delta = 0, \tag{30}$$

where $\delta = (\delta_{-1}, \delta_0, \ldots, \delta_N, \delta_{N+1})^T$ global element parameters. The A, B, C and λD matrices are rectangular and row m of each has the following form:

$$A = \frac{1}{60}(1, 57, 302, 302, 57, 1, 0), \quad B = \frac{1}{2}(-1, -9, 10, 10, -9, -1, 0),$$
$$C = (0, 0, 0, 0, 0, 0, 0)$$
$$\lambda D = \frac{1}{10}\begin{pmatrix} -\lambda_1, -12\lambda_1 - 13\lambda_2, 7\lambda_1 - 41\lambda_2 - 6\lambda_3, 6\lambda_1 + 41\lambda_2 - 7\lambda_3, \\ 13\lambda_2 + 12\lambda_3, \lambda_3 \end{pmatrix}$$

where

$$\lambda_1 = \frac{1 + p(p+1)}{2^p h}(\delta_{m-2} + 5\delta_{m-1} + 5\delta_m + \delta_{m+1})^p, \quad \lambda_2 = \frac{1 + p(p+1)}{2^p h}(\delta_{m-1} + 5\delta_m + 5\delta_{m+1} + \delta_{m+2})^p,$$
$$\lambda_3 = \frac{1 + p(p+1)}{2^p h}(\delta_m + 5\delta_{m+1} + 5\delta_{m+2} + \delta_{m+3})^p.$$

Replacing the time derivative $\dot{\delta}$ by the forward difference approximation $\dot{\delta} = (\delta^{n+1} - \delta^n)/\Delta t$ and the parameter δ by the Crank–Nicolson formulation $\delta = (1/2)(\delta^n + \delta^{n+1})$, then Equation (30) reduce to the following matrix system:

$$\left[A + \beta(B - C) + \frac{\lambda\Delta t}{2}D\right]\delta^{n+1} = \left[A + \beta(B - C) - \frac{\lambda\Delta t}{2}D\right]\delta^n \tag{31}$$

where t is time step. Applying the boundary conditions (5) to the system (31), $(N+1)\times(N+1)$ matrix system is obtained. This last system is actively solved with a variant of the Thomas algorithm but in solution process, two or three inner iterations $\delta^{n^*} = \delta^n + (1/2)(\delta^n - \delta^{n-1})$ are also practiced at each time step to overcome the non-linearity. Ultimately, a typical member of the matrix system (31) is written in terms of the nodal parameters δ^n and δ^{n+1} as:

$$\begin{aligned} &\gamma_1\delta_{m-2}^{n+1} + \gamma_2\delta_{m-1}^{n+1} + \gamma_3\delta_m^{n+1} + \gamma_4\delta_{m+1}^{n+1} + \gamma_5\delta_{m+2}^{n+1} + \gamma_6\delta_{m+3}^{n+1} \\ &= \gamma_6\delta_{m-2}^{n} + \gamma_5\delta_{m-1}^{n} + \gamma_4\delta_m^{n} + \gamma_3\delta_{m+1}^{n} + \gamma_2\delta_{m+2}^{n} + \gamma_1\delta_{m+3}^{n}, \end{aligned} \tag{32}$$

where

$$\gamma_1 = \frac{1}{60} - \frac{\beta}{2} - \frac{\lambda\Delta t}{20}, \quad \gamma_2 = \frac{57}{60} - \frac{9\beta}{2} - \frac{25\lambda\Delta t}{20}, \quad \gamma_3 = \frac{302}{60} + \frac{10\beta}{2} - \frac{40\lambda\Delta t}{20},$$
$$\gamma_4 = \frac{302}{60} + \frac{10\beta}{2} + \frac{40\lambda\Delta t}{20}, \quad \gamma_5 = \frac{57}{60} - \frac{9\beta}{2} + \frac{25\lambda\Delta t}{20}, \quad \gamma_6 = \frac{1}{60} - \frac{\beta}{2} + \frac{\lambda\Delta t}{20}.$$

To start the evolution of the vector of parameters δ^n, δ^0 must be calculated by using the periodic boundary and initial conditions $u(x, 0)$. So, using the relations at the knots $u_N(x_m, 0) = u(x_m, 0)$, $m = 0$, 1, 2, …, N and $u'_N(x_0, 0) = u'(x_N, 0) = 0$ together with a variant of algorithm by Thomas, the initial vector δ^0 is easily got from the following matrix equation

$$\begin{bmatrix} -3 & 0 & 3 & & & & \\ 1 & 4 & 1 & & & & \\ & & \ddots & & & & \\ & & & 1 & 4 & 1 & \\ & & & -3 & 0 & 3 & \end{bmatrix}\begin{bmatrix} \delta_{-1}^0 \\ \delta_0^0 \\ \vdots \\ \delta_N^0 \\ \delta_{N+1}^0 \end{bmatrix} = \begin{bmatrix} u'(x_0, 0) \\ u(x_0, 0) \\ \vdots \\ u(x_N, 0) \\ u'(x_N, 0) \end{bmatrix}.$$

5 | STABILITY ANALYSIS

In this section, like other authors [16, 23, 31, 32] our stability analysis is based on the Von Neumann theory in which the growth factor of a typical Fourier model defined as

$$\delta_j^n = g^n e^{ijkh}, \tag{33}$$

where k is mode number and h is element greatness. To implement the Fourier stability analysis, Equation (2) needs to be linearized by assuming that u^p in the nonlinear term $u^p u_x$ is locally constant. Substituting (33) into linearized scheme of (32), we get

$$g = \frac{a - ib}{a + ib}, \tag{34}$$

where

$$\begin{aligned} a &= (302 + 300\beta)\cos\left(\frac{\theta}{2}\right)h + (57 - 270\beta)\cos\left(\frac{3\theta}{2}\right)h + (1 - 30\beta)\cos\left(\frac{5\theta}{2}\right)h, \\ b &= 120\lambda\Delta t \sin\left(\frac{\theta}{2}\right)h + 75\lambda\Delta t \sin\left(\frac{3\theta}{2}\right)h + 3\lambda\Delta t \sin\left(\frac{5\theta}{2}\right)h, \end{aligned} \tag{35}$$

so that $|g|$ is 1 and our linearized scheme is neutrally stable.

6 | COMPUTER IMPLEMENTATIONS AND ILLUSTRATIONS

In this part, we introduce the results of the numerical experiments of our algorithm for the solution of the GRLW Equations (4) and (5) for a single solitary wave and an interaction of two solitary waves. We also display the development of the Maxwellian initial condition into solitary waves. In order to demonstrate how favorable our numerical algorithm foresees the position and amplitude of the solution as the simulation progresses, we provide for the following error norms:

$$L_2 = \|u^{exact} - u_N\|_2 \simeq \sqrt{h\sum_{J=0}^{N} |u_j^{exact} - (u_N)_j|^2},$$

and

$$L_\infty = \|u^{exact} - u_N\|_\infty \simeq \max_j |u_j^{exact} - (u_N)_j|.$$

With the boundary condition $u \to 0$ for $x \to \pm\infty$ the exact solution of the GRLW equation is [29]

$$u(x,t) = \sqrt[p]{\frac{c(p+2)}{2p}}\,\sec h^2\left[\frac{p}{2}\sqrt{\frac{c}{\mu(c+1)}}(x - (c+1)t - x_0)\right]$$

where $\sqrt[p]{\frac{c(p+2)}{2p}}$ is amplitude, $c+1$ is the speed of the wave traveling in the positive direction of the x-axis, x_0 is arbitrary constant. There are three conserved quantities

$$\begin{aligned} I_1 &= \int_{-\infty}^{\infty} u(x,t)dx, \\ I_2 &= \int_{-\infty}^{\infty} [u^2(x,t) + \mu u_x^2(x,t)]dx, \\ I_3 &= \int_{-\infty}^{\infty} [u^4(x,t) - \mu u^2(x,t)]dx \end{aligned} \tag{36}$$

for the GRLW equation. These are correspond to mass, momentum and energy respectively.

TABLE 1 Invariants and errors for single solitary wave with $p = 2$, $c = 1$, $h = 0.2$, $\Delta t = 0.025$, $\mu = 1$, $x \in [0, 100]$

Time	I_1	I_2	I_3	$L_2 \times 10^3$	$L_\infty \times 10^3$
0	4.442866	3.299813	1.414214	0.000000	0.000000
2	4.442940	3.299938	1.414330	1.948707	1.190456
4	4.443005	3.300033	1.414425	2.362855	1.222540
6	4.443068	3.30012	1.414515	2.449792	1.198936
8	4.443129	3.300213	1.414604	2.448242	1.150862
10	4.443175	3.300302	1.414692	2.415468	1.079686

TABLE 2 Comparisons of results for single solitary wave with $p = 2$, $c = 1$, $h = 0.2$, $\Delta t = 0.025$, $\mu = 1$, $x \in [0, 100]$

Method	I_1	I_2	I_3	$L_2 \times 10^3$	$L_\infty \times 10^3$
Analytic	4.44288	3.29983	1.41421	0.000000	0.000000
Our method	4.443175	3.300302	1.414692	2.415468	1.079686
Petrov–Galerkin [23]	4.44288	3.29981	1.41416	3.00533	1.68749
Septic collocation first scheme [25]	4.442866	3.299822	1.414204	2.632463	1.393064
Septic collocation second scheme [25]	4.442866	3.299715	1.414312	2.571481	1.340210
Cubic Galerkin [26]	3.801670	2.888066	0.979294	13.291080	8.478107
Cubic B-spline coll-CN [30]	4.442	3.299	1.413	16.39	9.24
Cubic B-spline coll + PA-CN [30]	4.440	3.296	1.411	20.3	11.2
Cubic B-spline collocation [31]	4.44288	3.29983	1.41420	9.30196	5.43718

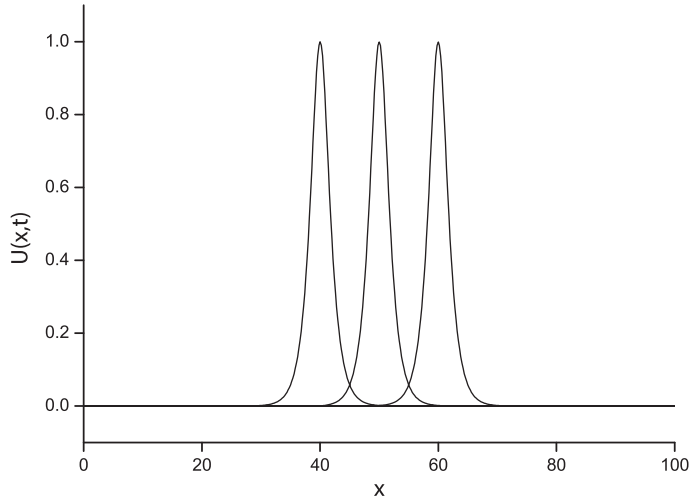

FIGURE 1 Motion of single solitary wave for $p = 2$, $c = 1$, $h = 0.2$, $\Delta t = 0.025$ over the interval [0, 100] at $t = 0, 5, 10$

6.1 | Dispersion of a single solitary wave

In our computational work for the first set, we prefer the parameters $p = 2$, $c = 1$, $h = 0.2$, $\Delta t = 0.025$, $\mu = 1$, $x_0 = 40$ with interval [0, 100] to match up with that of previous papers [23, 25, 26, 30, 31]. These values yield the amplitude 1.0 and the run of the algorithm is continued up to time $t = 10$ over the solution region. Analytical values of the invariants are $I_1 = 4.442883$, $I_2 = 3.299832$, and

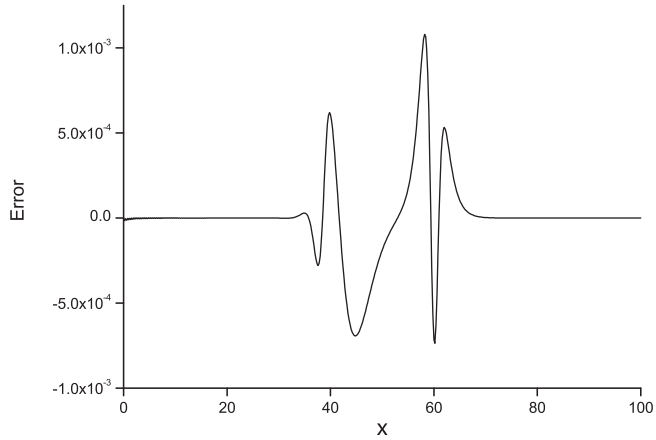

FIGURE 2 Error graph for $p = 2$, $c = 1$, $h = 0.2$, $\Delta t = 0.025$ at $t = 10$

TABLE 3 Invariants and errors for single solitary wave with $p = 3$, $c = 6/5$, $h = 0.1$, $\Delta t = 0.025$, $\mu = 1$, $x \in [0, 100]$

Time	I_1	I_2	I_3	$L_2 \times 10^3$	$L_\infty \times 10^3$
0	3.797185	2.881250	0.972968	0.000000	0.000000
2	3.797187	2.881258	0.973414	1.700682	1.174285
4	3.797187	2.881257	0.973473	2.805942	1.797229
6	3.797187	2.881255	0.973486	3.899300	2.428864
8	3.797200	2.881254	0.973487	5.007404	3.073644
10	3.797282	2.881293	0.973446	6.128029	3.722138

TABLE 4 Comparisons of results for single solitary wave with $p = 3$, $c = 6/5$, $h = 0.1$, $\Delta t = 0.025$, $\mu = 1$, $x \in [0, 100]$

Method	I_1	I_2	I_3	$L_2 \times 10^3$	$L_\infty \times 10^3$
Our method	3.797282	2.881293	0..973446	6.128029	3.722138
Petrov–Galerkin [23]	3.79713	2.88123	0.972243	7.76745	4.70875
Septic collocation first scheme [25]	3.797185	2.881252	0.973145	8.972983	5.175982
Septic collocation second scheme [25]	3.797133	2.881089	0.973128	7.778169	4.441873
Cubic Galerkin [26]	3.801670	2.888066	0.979294	13.291080	8.478107

$I_3 = 1.414214$. Values of the three invariants as well as L_2 and L_∞-error norms from our method have been computed and tabulated in Table 1. Referring to Table 1 the error norms L_2 and L_∞ remain less than 2.4154685×10^{-3} and $1.07968675 \times 10^{-3}$, the invariants I_1, I_2 and I_3 change from their initial values by less than 3.10×10^{-4}, 4.89×10^{-4}, and 4.79×10^{-4}, respectively, throughout the simulation. Also, our invariants are almost stable as time increases and the agreement between numerical and analytic solutions is perfect. Hence our method is acceptedly conservative. Comparisons with our results with exact solution as well as the obtained values in [23, 25, 26, 30, 31] have been made and listed in Table 2 at $t = 10$. This table evidentially indicates that the error norms got by our method are marginally less than the others. The motion of solitary wave using our scheme is plotted at time $t = 0, 5, 10$ in Figure 1. It is obvious from the figure that the suggested method performs the motion of propagation of a solitary wave admissibly, which moved to the right with the preserved amplitude and

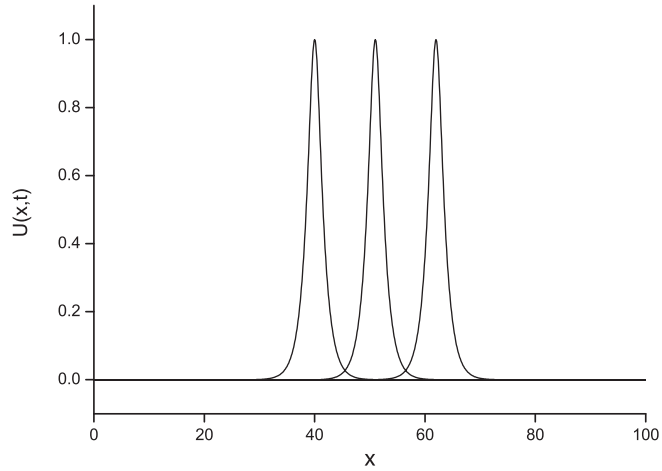

FIGURE 3 Motion of single solitary wave for $p = 3$, $c = 6/5$, $h = 0.1$, $\Delta t = 0.025$ over the interval [0, 100] at $t = 0, 5, 10$

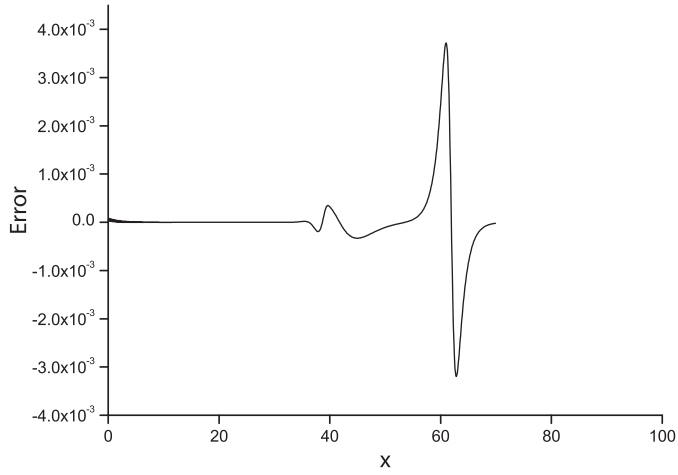

FIGURE 4 Error graph for $p = 3$, $c = 6/5$, $h = 0.1$, $\Delta t = 0.025$ at $t = 10$

shape. Initially, the amplitude of solitary wave is 1.00000 and its top position is pinpionted at $x = 40$. At $t = 10$, its amplitude is recorded as 0.99928 with center $x = 60$. Thereby the absolute difference in amplitudes over the time interval [0, 10] are observed as 7.16×10^{-3}. The quantile of error at discount times are depicted in Figure 2. The error aberration varies from -1×10^{-3} to 1×10^{-3}.

For the second set, we select the parameters $p = 3$, $c = 6/5$, $h = 0.1$, $\Delta t = 0.025$, $\mu = 1$, $x_0 = 40$ with interval [0, 100] to coincide with that of previous papers [23, 25, 26]. These parameters produce the amplitude 1.0 and the computations are carried out for times up to $t = 10$. The error norms L_2, L_∞ and conservation quantities I_1, I_2, and I_3 are computed, which are recorded in Table 3. According to Table 3 the error norms L_2 and L_∞ remain less than $6.12802937 \times 10^{-3}$ and $3.72213891 \times 10^{-3}$, the invariants I_1, I_2, and I_3 change from their initial values by less than 9.75×10^{-5}, 4.32×10^{-5}, and 4.78×10^{-4}, respectively, during the simulation. Also, our invariants are almost constant as time increases. Therefore our method is satisfactorily conservative. In Table 4 the performance of the our new method is compared with other methods [23, 25, 26] at $t = 10$. It is observed that errors of the

TABLE 5 Invariants and errors for single solitary wave with $p = 4$, $c = 4/3$, $h = 0.1$, $\Delta t = 0.01$, $\mu = 1$, $x \in [0, 100]$

Time	I_1	I_2	I_3	$L_2 \times 10^3$	$L_\infty \times 10^3$
0	3.468709	2.671691	0.729204	0.000000	0.000000
2	3.468718	2.671714	0..729969	0.967786	0.708600
4	3.468719	2.671714	0.730017	1.040242	0.591250
6	3.468720	2.671714	0.730027	1.102854	0.611363
8	3.468731	2.671714	0.730028	1.183442	0.715175
10	3.468799	2.671742	0.730001	1.283420	0.821650

TABLE 6 Comparisons of results for single solitary wave with $p = 4$, $c = 4/3$, $h = 0.1$, $\Delta t = 0.01$, $\mu = 1$, $x \in [0, 100]$

Method	I_1	I_2	I_3	$L_2 \times 10^3$	$L_\infty \times 10^3$
Our method	3.468799	2.671742	0..730001	1.283420	0.821650
Petrov–Galerkin [23]	3.46866	2.67168	0.728881	2.46065	1.56620
Septic collocation first scheme [25]	3.468709	2.671696	0.729258	3.351740	2.049733
Septic collocation second scheme [25]	3.468671	2.671658	0.729237	2.698709	1.656002
Cubic Galerkin [26]	3.470439	2.674445	0.731987	1.511394	0.857585

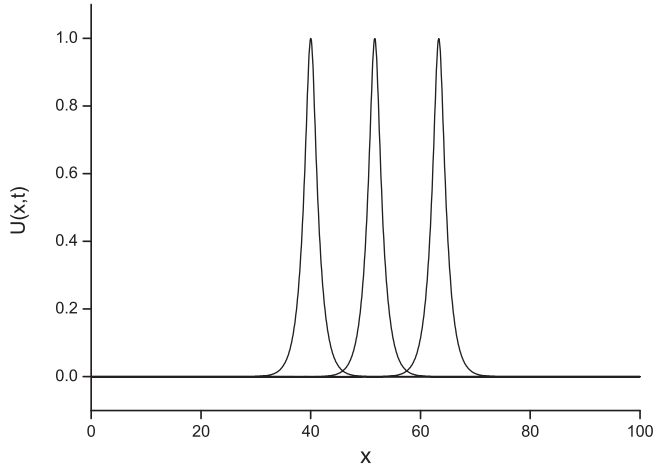

FIGURE 5 Motion of single solitary wave for $p = 4$, $c = 4/3$, $h = 0.1$, $\Delta t = 0.01$ over the interval [0, 100] at $t = 0, 5, 10$

method [23, 25, 26] are considerably larger than those obtained with the present scheme. Perspective views of the traveling solitons are graphed at time $t = 0, 5, 10$ in Figure 3. It is clear from the figure that the single soliton moved to the right with the preserved amplitude and shape. The amplitude is 1.00000 at $t = 0$ and located at $x = 40$, while it is 0.99958 at $t = 10$ and located at $x = 62$. The absolute difference in amplitudes over the time interval [0, 10] are found as 4.2×10^{-4}. The aberration of error at discrete times is modeled in Figure 4. The error deviation varies from -4×10^{-3} to 4×10^{-3}.

Finally, we choose the parameters $p = 4$, $c = 4/3$, $h = 0.1$, $\Delta t = 0.01$, $\mu = 1$, $x_0 = 40$ over the region [0, 100] to compare with those of earlier papers [23, 25, 26]. These parameters lead to amplitude 1.0 and the simulations are executed to time $t = 10$ to invent the error norms L_2 and L_∞ and the numerical invariants I_1, I_2 and I_3. For these values of the parameters, the conservation properties and

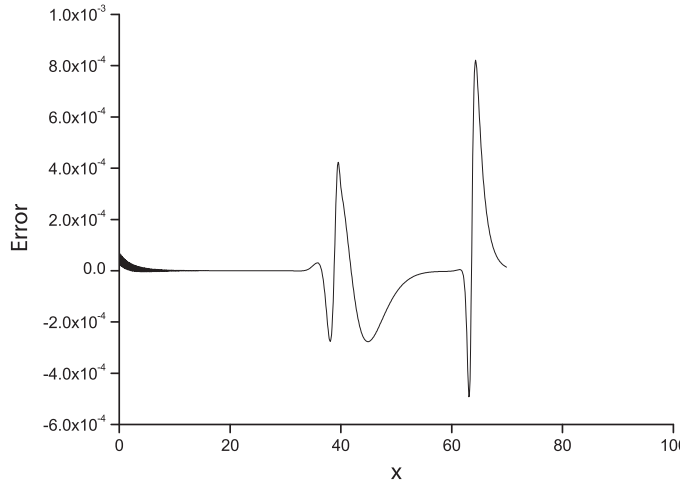

FIGURE 6 Error graph for $p = 4$, $c = 4/3$, $h = 0.1$, $\Delta t = 0.01$ at $t = 10$

TABLE 7 Invariants for interaction of two solitary waves with $p = 3$

	t	0	2	4	6
I_1	Our method	9.690777	9.690777	9.690777	9.690777
	[23]	9.69075	9.69074	9.69074	9.69074
	[25] First	9.690777	9.690777	9.690777	9.690778
	[25] Second	9.690777	9.688117	9.686015	9.683462
	[26]	9.6907	9.6906	9.6898	9.6901
I_2	Our method	12.944360	12.928161	12.957476	12.988509
	[23]	12.9444	12.9452	12.9453	12.9454
	[25] First	12.944391	12.944392	12.944393	12.944394
	[25] Second	12.944391	12.939062	12.970312	13.002753
	[26]	12.9443	12.9440	12.9418	12.9426
I_3	Our method	17.018706	17.034905	17.005590	16.974557
	[23]	17.0184	16.9835	16.9261	16.9113
	[25] First	17.018675	17.02567	16.981696	16.952024
	[25] Second	17.018675	17.02400	16.992754	16.960313
	[26]	17.0187	17.0324	16.9849	16.9557

the L_2-error as well as the L_∞-error norms have been given in Table 5 for various values of the time level t. It can be noted from Table 5 the error norms L_2 and L_∞ remain less than $1.28342020 \times 10^{-3}$ and $0.82165081 \times 10^{-3}$, the invariants I_1, I_2 and I_3 change from their initial values by less than 9.02×10^{-5}, 5.08×10^{-5}, and 7.97×10^{-4}, respectively, throughout the simulation. Also, our invariants are almost constant as time increases. Therefore we can say our method is sensibly conservative. The comparison between the results obtained by the present method with those in the other studies [23, 25, 26] is also documented in Table 6. It is noticeably seen from the table that errors of the present method are radically less than those obtained with the earlier schemes [23, 25, 26]. For visual representation, the simulations of single soliton for values $p = 4$, $c = 4/3$, $h = 0.1$, $\Delta t = 0.01$ at times $t = 0$, 5 and 10 are illustrated in Figure 5. It is understood from this figure that the numerical scheme performs the motion of propagation of a single solitary wave, which moves to the right at nearly unchanged speed and conserves its amplitude and shape with increasing time. The amplitude is 1.00000 at $t = 0$ and

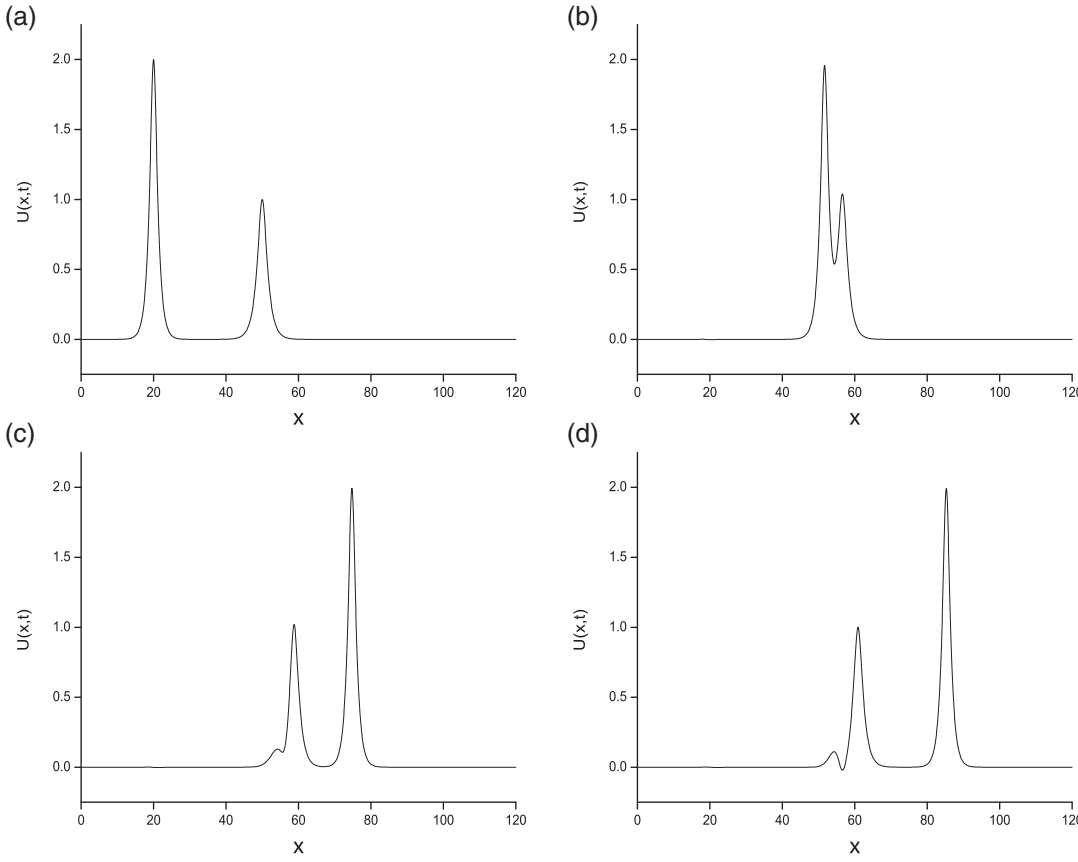

FIGURE 7 Interaction of two solitary waves at $p = 3$; (a) $t = 0$, (b) $t = 3$, (c) $t = 5$, (d) $t = 6$

located at $x = 40$, while it is 0.99892 at $t = 10$ and located at $x = 63.3$. The absolute difference in amplitudes at times $t = 0$ and $t = 10$ is 1.08×10^{-3} so that there is a little change between amplitudes. Error distributions at time $t = 10$ are shown graphically in Figure 6. As it is seen, the maximum errors are between -6×10^{-4} and 1×10^{-3} and occur around the central position of the solitary wave.

6.2 | Interaction of two solitary waves

As a second problem, we have focused on the behavior of the interaction of two solitary waves having different amplitudes and moving in the same direction. We provide for the GRLW equation with initial conditions given by the linear sum of two well separated solitary waves of various amplitudes

$$u(x,0) = \sum_{j=1}^{2} \sqrt[p]{\frac{c_j(p+2)}{2p}} \sec h^2 \left[\frac{p}{2} \sqrt{\frac{c_j}{\mu(c_j+1)}} (x - x_j) \right], \tag{37}$$

where c_j and x_j, $j = 1, 2$ are arbitrary constants. For the simulation, we firstly choose $p = 3$, $c_1 = 48/5$, $c_2 = 6/5$, $h = 0.1$, $\Delta t = 0.01$, $\mu = 1$ over the interval $0 \leq x \leq 120$. The amplitudes are in the ratio $2:1$. Calculations are performed to time $t = 6$. The results are listed in Table 7. Referring to this table, it is noticed that the numerical values of the invariants are very closed with the methods [23, 25, 26] during the computer run. The initial function was placed with the larger wave to the left of the smaller one as seen in Figure 7a. Both waves move to the right with velocities dependent upon their magnitudes.

TABLE 8 Invariants for interaction of two solitary waves with $p = 4$

	t	0	2	4	6
I_1	Our method	8.834272	8.834272	8.834272	8.834272
	[23]	8.83427	8.84204	8.84209	8.83434
	[25] First	8.834272	8.834160	8.834053	8.8339467
	[25] Second	8.834272	8.564186	8.435464	8.327161
	[26]	8.8342	8.7089	8.6518	8.6134
I_2	Our method	12.170706	11.339311	11.209384	15.812521
	[23]	12.1697	12.3700	12.5703	12.6103
	[25] First	12.170887	12.170537	12.170205	12.169873
	[25] Second	12.170887	11.939598	11.977097	11.814722
	[26]	12.1707	11.7871	11.6179	11.4992
I_3	Our method	14.029604	14.860999	14.990927	10.387789
	[23]	14.0302	13.9607	13.9805	14.6974
	[25] First	14.029423	14.413442	14.351624	14.292901
	[25] Second	14.029423	14.260712	14.223214	14.385588
	[26]	14.0296	12.9204	12.1972	11.9640

According to Figure 7, the larger wave catches up with the smaller wave at about $t = 3$, the overlapping process continues until $t = 4$, then two solitary waves emerge from the interaction and resume their former shapes and amplitudes. At $t = 6$, the magnitude of the smaller wave is 1.00029 on reaching position $x = 60.0$, and of the larger wave 1.99213 having the position $x = 85.3$, so that the difference in amplitudes is 0.00029 for the smaller wave and 0.00787 for the larger wave. The changes of the invariants for this case are satisfactorily small. Second, to ensure an interaction of two solitary waves take place, calculation is carried out with the parameters $p = 4$, $c_1 = 64/3$, $c_2 = 4/3$, $h = 0.125$, $\Delta t = 0.01$, $\mu = 1$ over the interval $0 \leq x \leq 200$. The parameters give solitary waves of different amplitudes 2 and 1 having centers at $x_1 = 20$ and $x_2 = 80$. The results are given in Table 8. According to the this table, it is realized that the numerical values of the invariants are very closed with the methods [23, 25, 26] during the computer run. The initial function was placed with the larger wave to the left of the smaller one as seen in Figure 8a. Both waves move to the right with velocities dependent upon their magnitudes. According to Figure 8, the larger wave catches up with the smaller wave at about $t = 3$, the overlapping process continues until $t = 5$, then two solitary waves emerge from the interaction and resume their former shapes and amplitudes.

6.3 | The Maxwellian initial condition

Finally, we have examined the evolution of an initial Maxwellian pulse into solitary waves, arising as initial condition

$$u(x, 0) = \exp(-(x - 40)^2). \tag{38}$$

For this problem, the behavior of the solution depends on the value of μ [13, 23]. Therefore, we chose the values of $\mu = 0.1$, $\mu = 0.05$, and $\mu = 0.025$ for $p = 2, 3, 4$. The numerical computations are done up to $t = 0.05$. Calculated numerical invariants at different values of t are shown in Table 9 and it is seen that calculated invariant values are satisfactorily constant. For $p = 2$ and $\mu = 0.1$; the variation of invariants I_1, I_2, and I_3 from initial variants changes less than 1.02×10^{-3}, 4.48×10^{-3}, and

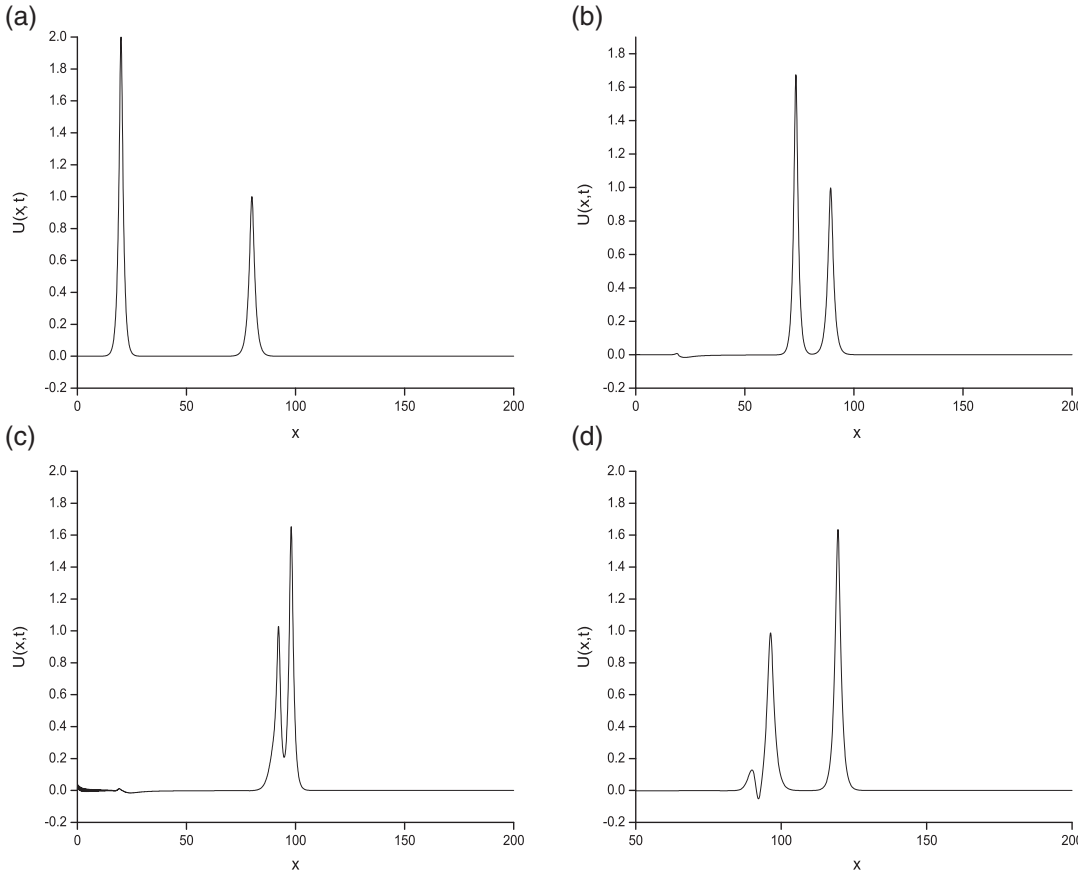

FIGURE 8 Interaction of two solitary waves at $p = 4$; (a) $t = 0$, (b) $t = 2$, (c) $t = 4$, (d) $t = 6$

8.69×10^{-3}%, respectively, and for $\mu = 0.05$; 2.01×10^{-3}, 8.35×10^{-3}, and 17.92×10^{-3}%, respectively, and for $\mu = 0.025$; 3.19×10^{-3}, 12.72×10^{-3}, and 29.28×10^{-3}%, respectively, for $p = 3$ and $\mu = 0.1$; the variation of invariants I_1, I_2 and I_3 from initial variants changes less than 8.60×10^{-3}, 2.77×10^{-2}, and 4.75×10^{-1}%, respectively, and for $\mu = 0.05$; 17.45×10^{-3}, 54.32×10^{-3}, and 6.62×10^{-1}%, respectively, and for $\mu = 0.025$; 30.92×10^{-3}, 93.27×10^{-3}, and 7.72×10^{-1}%, respectively, for $p = 4$ and $\mu = 0.1$; the variation of invariants I_1, I_2, and I_3 from initial variants changes less than 38.82×10^{-3}, 1.09×10^{-3} and 1.76%, respectively, and for $\mu = 0.05$; 67.23×10^{-3}, 1.99×10^{-1} and 2.48%, respectively, and for $\mu = 0.025$; 1.04×10^{-1}, 3.31×10^{-1}, and 3.0%, respectively. The development of the Maxwellian initial condition into solitary waves is shown in Figure 9.

7 | CONCLUSION

In this work, a numerical technique based on a Petrov–Galerkin method using quadratic weight functions and cubic B-spline finite elements has been proffered to get numerical solutions of GRLW equation. We experimented our algorithm along with single solitary wave in which the exact solution is known and broadened it to examine the interaction of two solitary waves and Maxwellian initial condition where the exact solutions are unknown during the interaction. Variational formulation and semi-discrete Galerkin scheme of the equation are generated. Stability analysis have been done and the

TABLE 9 Maxwellian initial condition for different values of μ

		$p = 2$			$p = 3$			$p = 4$		
μ	t	I_1	I_2	I_3	I_1	I_2	I_3	I_1	I_2	I_3
0.1	0.01	1.772481	1.378659	0.760911	1.772481	1.378655	0.760779	1.772422	1.378551	0.760310
	0.03	1.772475	1.378639	0.760890	1.772435	1.378538	0.759621	1.772189	1.378049	0.755954
	0.05	1.772463	1.378599	0.760847	1.772328	1.378278	0.757292	1.771793	1.377149	0.747477
0.05	0.01	1.772480	1.315994	0.823572	1.772480	1.315988	0.823384	1.772382	1.315812	0.822659
	0.03	1.772469	1.315959	0.823526	1.772388	1.315772	0.821657	1.771994	1.314976	0.816132
	0.05	1.772445	1.315887	0.823429	1.772171	1.315282	0.818116	1.71289	1.313372	0.803134
0.025	0.01	1.772480	1.284661	0.854901	1.772478	1.284651	0.854699	1.772340	1.284399	0.853806
	0.03	1.772462	1.284610	0.854823	1.772317	1.284299	0.852665	1.771760	1.283154	0.846013
	0.05	1.772424	1.284502	0.854658	1.771933	1.283467	0.848301	1.770623	1.280410	0.829240

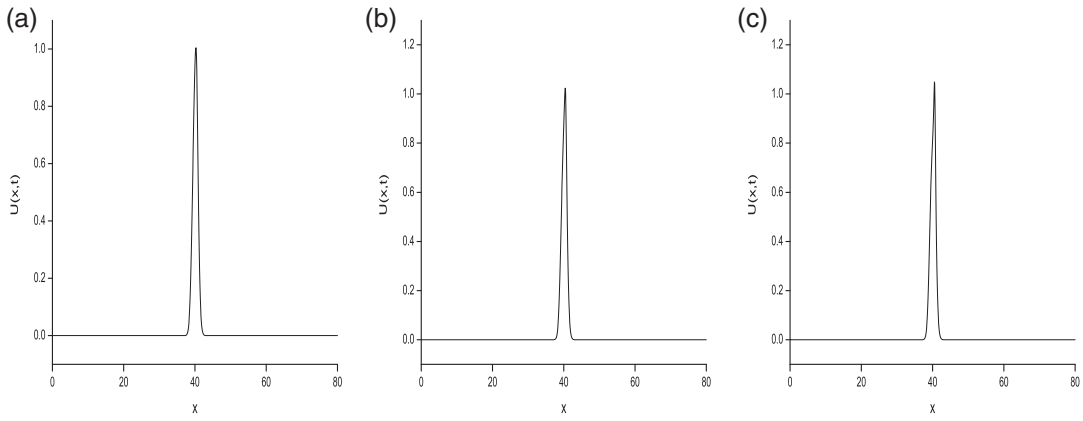

FIGURE 9 Maxwellian initial condition at $t = 0.05$ (a) $p = 2$, $\mu = 0.025$, (b) $p = 3$, $\mu = 0.025$, (c) $p = 4$, $\mu = 0.025$

linearized numerical scheme have been obtained unconditionally stable. The accuracy of the method is investigated both L_2 and L_∞ error norms and the invariant quantities I_1, I_2 and I_3. The obtained numerical results indicate that the error norms are satisfactorily small and the conservation laws are marginally constant in all computer program run. We can see that our numerical scheme for the equation is more accurate than the other earlier schemes found in the literature. Therefore, our numerical technique is suitable for getting numerical solutions of partial differential equations.

ORCID

Samir Kumar Bhowmik https://orcid.org/0000-0003-1599-5082

REFERENCES

[1] D. H. Peregrine, *Calculations of the development of an undular bore*, J. Fluid Mech. vol. 25 (1996) pp. 321–330.
[2] D. H. Peregrine, *Long waves on a beach*, J. Fluid Mech. vol. 27 (1967) pp. 815–827.
[3] T. B. Benjamin, J. L. Bona, J. J. Mahony, *Model equations for waves in nonlinear dispersive systems*, Philos. Trans. R. Soc. Lond. vol. 227 (1972) pp. 47–78.
[4] J. L. Bona, W. G. Pritchard, L. R. Scott, "*A comparison of solutions of two model equations for long waves*," in *Fluid dynamics in astrophysics and geophysics. Lectures in applied mathematics*, vol. 20, N. R. Lebovitz (Editor), American Mathematical Society, Providence, RI, 1983, pp. 235–267.

[5] J. L. Bona, W. G. Pritchard, L. R. Scott, *An evaluation of a model equation for water waves*, Philos. Trans. R. Soc. Lond., A vol. 302 (1981) pp. 457–510.

[6] J. L. Bona, P. J. Bryant, *A mathematical model for long waves generated by wave makers in nonlinear dispersive systems*, Proc. Camb. Philos. Soc. vol. 73 (1973) pp. 391–405.

[7] J. C. Eilbeck, G. R. McGuire, *Numerical study of the regularized long wave equation. II: Interaction of solitary wave*, J. Comp. Phys. vol. 23 (1977) pp. 63–73.

[8] P. C. Jain, R. Shankar, T. V. Singh, *Numerical solution of regularized long-wave equation*, Commun. Numer. Methods Eng. vol. 9 (1993) pp. 579–586.

[9] D. Bhardwaj, R. Shankar, *A computational method for regularized long wave equation*, Comp. Math. Appl. vol. 40 (2000) pp. 1397–1404.

[10] Q. Chang, G. Wang, B. Guo, *Conservative scheme for a model of nonlinear dispersive waves and its solitary waves induced by boundary motion*, J. Comput. Phys. vol. 93 (1995) pp. 360–375.

[11] B. Y. Gou, W. M. Cao, *The Fourier pseudospectral method with a restrain operator for the RLW equation*, J. Comput. Phys. vol. 74 (1988) pp. 110–126.

[12] S. Islam, S. Haq, A. Ali, *A meshfree method for the numerical solution of RLW equation*, J. Comput. Appl. Math. vol. 223 (2009) pp. 997–1012.

[13] D. Kaya, *A numerical simulation of solitary-wave solutions of the generalized regularized long-wave equation*, Appl. Math. Comput. vol. 149 (2004) pp. 833–841.

[14] M. E. Alexander, J. L. Morris, *Galerkin method applied to some model equations for nonlinear dispersive waves*, J. Comput. Phys. vol. 30 (1979) pp. 428–451.

[15] I. Dag, M. N. Özer, *Approximation of RLW equation by least square cubic B-spline finite element method*, Appl. Math. Model. vol. 25 (2001) pp. 221–231.

[16] A. Esen, S. Kutluay, *Application of a lumped Galerkin method to the regularized long wave equation*, Appl. Math. Comput. vol. 174 (2006) pp. 833–845.

[17] S. K. Bhowmik et al., *Solving exterior 2D Dirichlet problem for second order elliptic equations by inverted finite elements method*, Comput. Math. Appl. vol. 72(9) (2016) pp. 2315–2333.

[18] J. L. Bona, A. Soyeur, *On the stability of solitary wave solutions of model equations for long waves*, J. Nonlinear Sci. vol. 4 (1994) pp. 449–470.

[19] S. Hamdi et al., *Exact solutions and invariants of motion for general types of regularized long wave equations*, Math. Comput. Simul. vol. 65 (2004) pp. 535–545.

[20] J. I. Ramos, *Solitary wave interactions of the GRLW equation*, Chaos Solitons Fract. vol. 33 (2007) pp. 479–491.

[21] L. M. Zhang, *A finite difference scheme for generalized long wave equation*, Appl. Math. Comput. vol. 168 (2005) pp. 962–972.

[22] D. Kaya, S. M. El-Sayed, *An application of the decomposition method for the generalized KdV and RLW equations*, Chaos Solitons Fract. vol. 17 (2003) pp. 869–877.

[23] T. Roshan, *A Petrov–Galerkin method for solving the generalized regularized long wave (GRLW) equation*, Comput. Math. Appl. vol. 63 (2012) pp. 943–956.

[24] J. F. Wang, F. N. Bai, Y. M. Cheng, *A meshless method for the nonlinear generalized regularized long wave equation*, Chin. Phys. B vol. 20(3) (2011) p. 030206.

[25] S. B. G. Karakoç, H. Zeybek, *Solitary-wave solutions of the GRLW equation using septic B-spline collocation method*, Appl. Math. Comput. vol. 289 (2016) pp. 159–171.

[26] H. Zeybek, S. B. G. Karakoç, *A numerical investigation of the GRLW equation using lumped Galerkin approach with cubic B-spline*, Springer Plus vol. 5 (2016) p. 199.

[27] A. A. Soliman, *Numerical simulation of the generalized regularized long wave equation by He's variational iteration method*, Math. Comput. Simul. vol. 70 (2005) pp. 119–124.

[28] R. Mokhtari, M. Mohammadi, *Numerical solution of GRLW equation using sinc-collocation method*, Comput. Phys. Commun. vol. 181 (2010) pp. 1266–1274.

[29] C. M. Garcia-Lopez, J. I. Ramos, *Effects of convection on a modified GRLW equation*, Appl. Math. Comput. vol. 219 (2012) pp. 4118–4132.

[30] L. R. T. Gardner et al., *Approximations of solitary waves of the MRLW equation by b-spline finite element*, Arab. J. Sci. Eng. vol. 22 (1997) pp. 183–193.

[31] A. K. Khalifa, K. R. Raslan, H. M. Alzubaidi, *A collocation method with cubic b-splines for solving the MRLW equation*, J. Comput. Appl. Math. vol. 212(2) (2008) pp. 406–418.

[32] K. R. Raslan, T. S. EL-Danaf, *Solitary waves solutions of the MRLW equation using quintic b-splines*, J. King Saud Univ. Sci. vol. 22(3) (2010) pp. 161–166.

[33] F. Haq, S. Islam, I. A. Tirmizi, *A numerical technique for solution of the MRLW equation using quartic b-splines*, Appl. Math. Model. vol. 34(12) (2010) pp. 4151–4160.

[34] I. Dag, D. Irk, M. Sari, *The extended cubic b-spline algorithm for a modified regularized long wave equation*, Chin. Phys. B vol. 22(4) (2013) pp. 1674–1056.

[35] S. B. G. Karakoç, N. M. Yagmurlu, Y. Ucar, *Numerical approximation to a solution of the modified regularized long wave equation using quintic b-splines*, Bound. Value Probl. vol. 2013(1) (2013) p. 27.

[36] S. B. G. Karakoç, T. Ak, H. Zeybek, *An efficient approach to numerical study of the MRLW equation with b-spline collocation method*, Abstr. Appl. Anal. vol. 2014 (2014) pp. 1–15.
[37] A. Ghiloufi, A. Rouatbi, K. Omrani, *A new conservative fourth-order accurate difference scheme for solving a model of nonlinear dispersive equations*, Numer. Methods Part. Differ. Eq. vol. 41(13) (2018) pp. 5230–5253.
[38] A. Ghiloufi, K. Omrani, *New conservative difference schemes with fourth-order accuracy for some model equation for nonlinear dispersive waves*, Numer. Methods Part. Differ. Eq. vol. 34(2) (2018) pp. 451–500.
[39] T. Achouria, N. Khiaria, K. Omrani, *On the convergence of difference schemes for the Benjamin–Bona–Mahony (BBM) equation*, Appl. Math. Comput. vol. 182(2) (2006) pp. 999–1005.
[40] T. Achouri, K. Omrani, *Application of the homotopy perturbation method to the modified regularized long wave equation*, Numer. Methods Part. Differ. Eq. vol. 26(2) (2009) pp. 399–411.
[41] A. Rouatbi, T. Achouri, K. Omrani, *High-order conservative difference scheme for a model of nonlinear dispersive equations*, Comp. Appl. Math. vol. 37 (2018) pp. 4169–4195.
[42] A. Rouatbi, K. Omrani, *Two conservative difference schemes for a model of nonlinear dispersive equations*, Chaos Solitons Fract. vol. 104 (2017) pp. 516–530.
[43] S. B. G. Karakoc, S. K. Bhowmik, *Galerkin finite element solution for Benjamin–Bona–Mahony–Burgers equation with cubic B-splines*, Comput. Math. Appl. vol. 77 (2019) pp. 1917–1932.
[44] S. K. Bhowmik, S. B. G. Karakoc, *Numerical solutions of the generalized equal width wave equation using Petrov Galerkin method*. arXiv preprint arXiv:1904.05145.
[45] N. Atouani, K. Omrani, *Galerkin finite element method for the Rosenau–RLW equation*, Comput. Math. Appl. vol. 66(3) (2013) pp. 289–303.
[46] P. G. Ciarlet, *The finite element method for elliptic problems*, Soc. Ind. Appl. Math. (2002).
[47] V. Thomée, "*Galerkin finite element methods for parabolic problems*," in *Springer series in computational mathematics*, Springer, Berlin, 1997.
[48] P. M. Prenter, *Splines and variational methods*, John Wiley & Sons, New York, 1975.

How to cite this article: Bhowmik SK, Karakoc SBG. Numerical approximation of the generalized regularized long wave equation using Petrov–Galerkin finite element method. *Numer Methods Partial Differential Eq.* 2019;35:2236–2257. https://doi.org/10.1002/num.22410